Abiotic methane synthesis and serpentinization in olivine-hosted fluid inclusions

Frieder Klein[a,1], Niya G. Grozeva[b], and Jeffrey S. Seewald[a]

[a]Department of Marine Chemistry and Geochemistry, Woods Hole Oceanographic Institution, Woods Hole, MA 02543; and [b]Massachusetts Institute of Technology–Woods Hole Oceanographic Institution Joint Program in Oceanography, Cambridge, MA 02139

Edited by Kenneth A. Farley, California Institute of Technology, Pasadena, CA, and approved July 22, 2019 (received for review May 6, 2019)

The conditions of methane (CH_4) formation in olivine-hosted secondary fluid inclusions and their prevalence in peridotite and gabbroic rocks from a wide range of geological settings were assessed using confocal Raman spectroscopy, optical and scanning electron microscopy, electron microprobe analysis, and thermodynamic modeling. Detailed examination of 160 samples from ultraslow- to fast-spreading midocean ridges, subduction zones, and ophiolites revealed that hydrogen (H_2) and CH_4 formation linked to serpentinization within olivine-hosted secondary fluid inclusions is a widespread process. Fluid inclusion contents are dominated by serpentine, brucite, and magnetite, as well as $CH_{4(g)}$ and $H_{2(g)}$ in varying proportions, consistent with serpentinization under strongly reducing, closed-system conditions. Thermodynamic constraints indicate that aqueous fluids entering the upper mantle or lower oceanic crust are trapped in olivine as secondary fluid inclusions at temperatures higher than ∼400 °C. When temperatures decrease below ∼340 °C, serpentinization of olivine lining the walls of the fluid inclusions leads to a near-quantitative consumption of trapped liquid H_2O. The generation of molecular H_2 through precipitation of Fe(III)-rich daughter minerals results in conditions that are conducive to the reduction of inorganic carbon and the formation of CH_4. Once formed, $CH_{4(g)}$ and $H_{2(g)}$ can be stored over geological timescales until extracted by dissolution or fracturing of the olivine host. Fluid inclusions represent a widespread and significant source of abiotic CH_4 and H_2 in submarine and subaerial vent systems on Earth, and possibly elsewhere in the solar system.

abiotic methane | fluid inclusions | serpentinization | methane seeps | carbon cycling

The formation of molecular hydrogen (H_2) and abiotic hydrocarbons such as methane (CH_4) has far-reaching implications for our understanding of the deep Earth carbon cycle, as well as the origin and maintenance of life on Earth and beyond. Elevated concentrations of H_2 and CH_4 are associated with the hydrous alteration of olivine-rich (ultramafic) rocks in many natural environments, a process that entails a number of redox-dependent dissolution–precipitation reactions collectively known as serpentinization. Large quantities of H_2 are generated during aqueous oxidation of ferrous iron-bearing minerals which results in the reduction of dissolved inorganic carbon ($\sum CO_2 = CO_{2(aq)} + H_2CO_3 + HCO_3^- + CO_3^{2-}$). Due to its important roles in a broad array of biogeochemical processes, few aspects of deep-sea hydrothermal vent systems and alkaline springs and gas seeps on land have attracted more attention than the origin of abiotic CH_4 (1–5). Field observations have revealed that the abundance of abiotic CH_4 in hydrothermal systems hosted in mafic rocks (basalt, diabase, gabbro) is substantially lower than in hydrothermal systems hosted in ultramafic rocks (peridotite or peridotite plus gabbro), but the pathways of abiotic CH_4 synthesis have remained elusive. Recently, McDermott et al. (3) used carbon isotopic and mass balance constraints to demonstrate that $\sum CO_2$ reduction by H_2 does not yield CH_4 during convection of hydrothermal fluids at the Von Damm hydrothermal field, suggesting that abiotic CH_4 formation and convective seawater circulation are decoupled. This challenged the paradigm of significant abiotic CH_4 formation during active fluid circulation and led to the suggestion that abiotic CH_4 observed in deep-sea hydrothermal fluids associated with ultramafic rocks may be leached from fluid inclusions (3, 6–8). Many important questions remain regarding fluid inclusion prevalence, formation, internal fluid–mineral interaction, and their contributions of CH_4 to venting fluids and global reservoirs. Moreover, because fluid inclusions may form in olivine-rich rocks that interact with water on celestial bodies elsewhere in our solar system, their formation may have key implications for the maintenance of microbial life beyond Earth.

Here we examined the chemical and mineralogical composition of fluid inclusions in olivine-bearing gabbros and partially serpentinized peridotites from ultraslow-, slow-, and fast-spreading midocean ridges, a backarc basin, subduction zone forearcs, and ophiolites (Fig. 1 and *SI Appendix*, Table S1). We assessed the distribution and composition of secondary fluid inclusions in olivine by means of confocal Raman spectroscopy, scanning electron microscopy, transmitted and reflected light microscopy, and electron microprobe analysis. Complementing these efforts, we used thermodynamic reaction path models to assess the geochemical environments present within the inclusions during fluid entrapment, serpentinization, and CH_4 formation.

Methane Abundance in Oceanic Peridotite and Gabbro

Examination of gabbro ($n = 43$) and peridotite ($n = 117$) in thin sections with relict olivine revealed the presence of fluid inclusions in rocks from each of the field locations shown in Fig. 1. All of the olivine-bearing gabbro samples and 77% of the peridotite samples contain fluid inclusions hosted in olivine. Image analyses of some of the most inclusion-rich samples revealed more than 3×10^6 inclusions per cm^3. Inclusions vary in size from <100 nm to ∼30 μm in diameter and are heterogeneously distributed on a millimeter to centimeter scale (Figs. 2 and 3 and *SI Appendix*,

Significance

Our findings highlight the ubiquitous occurrence of methane (CH_4)-rich fluid inclusions in olivine-bearing rocks that, collectively, may constitute one of the largest reservoirs of abiotic CH_4 on Earth. Because serpentinization in olivine-hosted fluid inclusions takes place in isolation from the surrounding rock, hydrogen (H_2) and CH_4 can form in any rock type containing olivine that hosts aqueous fluid inclusions, including those that do not undergo serpentinization on a macroscopic scale. Serpentinization and associated CH_4 formation within olivine-hosted fluid inclusions has likely supplied microbial ecosystems with abiotic CH_4 throughout most of Earth's history and may be a source of H_2 and CH_4 on other planetary bodies in our solar system, even those where liquid water is no longer present.

Author contributions: F.K., N.G.G., and J.S.S. designed research, performed research, analyzed data, and wrote the paper.

The authors declare no conflict of interest.

This article is a PNAS Direct Submission.

[1]To whom correspondence may be addressed. Email: fklein@whoi.edu.

This article contains supporting information online at www.pnas.org/lookup/suppl/doi:10.1073/pnas.1907871116/-/DCSupplemental.

Published online August 19, 2019.

Figs. S1, S3, and S4). Most inclusions occur along planes, which indicate a secondary origin via annealing of fluid-filled fractures in the olivine host (9, 10). With the exception of 3 sites, i.e., Hess Deep, the Romanche Fracture Zone, and the Mid-Atlantic Ridge Kane Fracture Zone Area (MARK) which do not contain detectable CH_4 in olivine-hosted fluid inclusions despite being rich in H_2, olivine-hosted fluid inclusions from all other sites examined in this study contain $CH_{4(g)}$ or $CH_{4(g)}$ and $H_{2(g)}$ (Figs. 1 and 3 and *SI Appendix*, Figs. S1 and S2 and Table S1). The partial pressure of $CH_{4(g)}$ within olivine-hosted fluid inclusions determined using empirical calibrations of the Raman shifts of $CH_{4(g)}$ (11) (*SI Appendix*, Table S1) are 0.4 to 55 MPa, with an average of 11.5 MPa. Using the ideal gas law and the assumption that fluid inclusions are spherical, we calculated that an inclusion with a diameter of 10 μm contains 8.4×10^{-5} to 1.2×10^{-2} nmol $CH_{4(g)}$.

The $CH_{4(g)}$ content of individual fluid inclusions can be used in conjunction with their abundance to estimate the $CH_{4(g)}$ content of olivine-rich rocks. A rock containing 10^5 inclusions per cm^3 would contain 2.5 to 363 nmol $CH_{4(g)}$ per gram of olivine. For comparison, recent whole rock analyses of partially serpentinized peridotite from the Mid-Cayman Rise and the Zambales ophiolite indicate minimum $CH_{4(g)}$ contents of 2 to 37 nanomoles (nmol) per gram of rock (6). If it is assumed that peridotite constitutes at least 5% of the seafloor in the Atlantic (12), Arctic, and Indian Oceans, and that 77% of the peridotite contains 75 wt. % olivine with fluid-inclusion–hosted CH_4 concentrations of 2.5 to 363 nmol $CH_{4(g)}$ per gram of olivine, we calculated that the uppermost kilometer of mantle peridotite at slow- and ultraslow-spreading ridges contains a combined mass of 2.5 to 367 Tg $CH_{4(g)}$ globally. Note that this minimum estimate does not include peridotite at passive margins, subduction zone forearcs, fast-spreading ridges, and ophiolites, which may contain additional CH_4.

The lower oceanic crust likely represents an even larger reservoir of abiotic CH_4 than the upper mantle. Gabbro is the dominant rock type in the lower oceanic crust (12) and, as the present study demonstrates, olivine in gabbro can contain abundant $CH_{4(g)}$-rich secondary fluid inclusions. Grozeva et al. (6) reported minimum concentrations of 72 to 310 nmol $CH_{4(g)}$ per gram of gabbro in fluid inclusions hosted in olivine, plagioclase, and clinopyroxene. If we assume that gabbro occurs in least 50% of the area in the Atlantic, Arctic, and Indian Oceans, that gabbro contains at least 72 nmol $CH_{4(g)}$ g^{-1} (6), and that the thickness of the gabbro layer at slow-spreading ridges, although highly variable, is close to 4 km on average (13, 14), the total amount of $CH_{4(g)}$ contained in the lower oceanic crust is on the order of 4.8 Pg. Combining this value with CH_4 stored in upper-mantle peridotite suggests that the fluid-inclusion–hosted lithospheric CH_4 reservoir created at slow- and ultraslow-spreading midocean ridges exceeds the amount of preindustrial CH_4 in the atmosphere (~2 Pg) (15). This estimate does not include the potential contribution of CH_4 hosted in fluid inclusions in the faster-spreading Pacific lithosphere. Our analysis of 2 sites in the Pacific (Hess Deep and Cocos Plate) yield contrasting results, which precludes a meaningful assessment at this point. However, the oceanic lithosphere in the Pacific contains additional, potentially massive amounts of abiotic CH_4 that remain to be quantified when more gabbro and peridotite samples from layered oceanic crust become available.

Serpentinization and $CH_{4(g)}$ Formation within Olivine-Hosted Fluid Inclusions

Electron microscope and confocal Raman analyses indicate that iron-bearing serpentine (chrysotile, lizardite, antigorite), iron-bearing brucite, and magnetite daughter minerals line the walls and occupy the interiors of fluid inclusions while the pore space is occupied by $H_{2(g)}$ or $CH_{4(g)}$, or both (Fig. 3 and *SI Appendix*, Figs. S1–S5 and Table S2). The dominant assemblage serpentine-brucite-magnetite-$H_{2(g)}$-$CH_{4(g)}$ provides robust evidence for serpentinization of the olivine interior under closed-system conditions (16). This assemblage is not limited to olivine-hosted fluid inclusions in ultramafic rocks, but is also common in olivine-hosted fluid inclusions in gabbroic rocks, indicating that serpentinization occurs in a wide range of protoliths. While no liquid water was detected in any of the inclusions examined, liquid water must have been present at the time of entrapment and was subsequently consumed by the formation of hydrous minerals at the expense of the olivine host. Accessory daughter minerals (typically <5 vol. %) detected in some inclusions include calcite, dolomite, magnesite, pentlandite, awaruite, talc, sylvite, and halite (*SI Appendix*, Fig. S4). Since dissolution of olivine can only contribute Mg, Fe, Si, and minor amounts of Ni and Ca for subsequent mineral formation, the presence of these accessory minerals indicates that trapped fluids contained additional of Na, K, Cl, S, and C. Furthermore, the occurrence of talc in some inclusions points to elevated concentrations of dissolved Si in the fluid from which it precipitated. Dissolved Si was likely derived from interaction of fluids with the host rock prior to fluid inclusion formation. Although the origin of the trapped fluids cannot be unequivocally determined, the presence of Na, K, and Cl is consistent with a seawater-like source fluid. Indeed, fluid-inclusion–bearing rocks from the Mid-Cayman Rise (*SI Appendix*, Table S1) have oxygen isotope

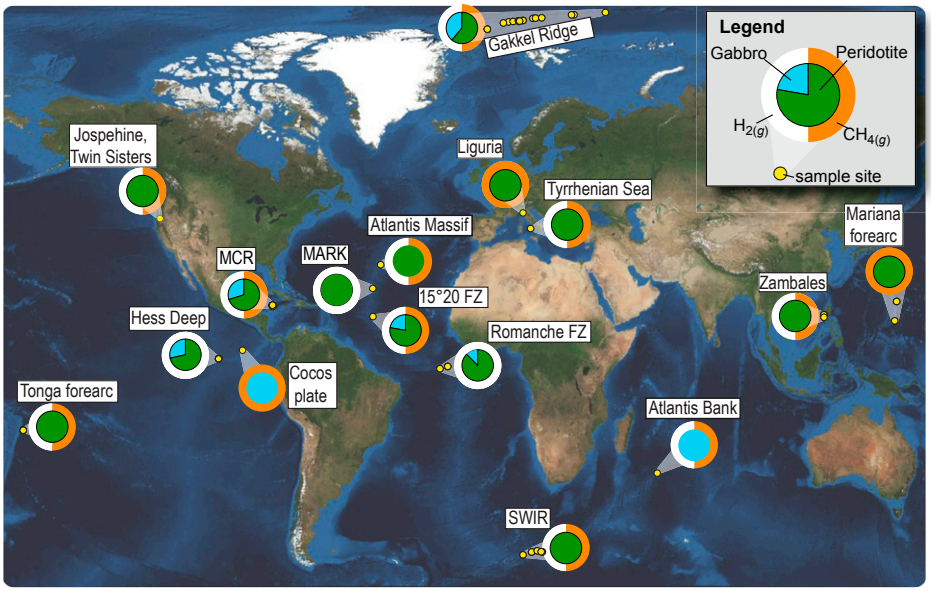

Fig. 1. Map showing the distribution, host rock type, and volatile contents of samples examined in this study. Note that inner circle of pie chart indicates proportions of olivine and gabbro whereas the color of the outer circle indicates the presence (or absence) of $H_{2(g)}$ (white) and $CH_{4(g)}$ (orange).

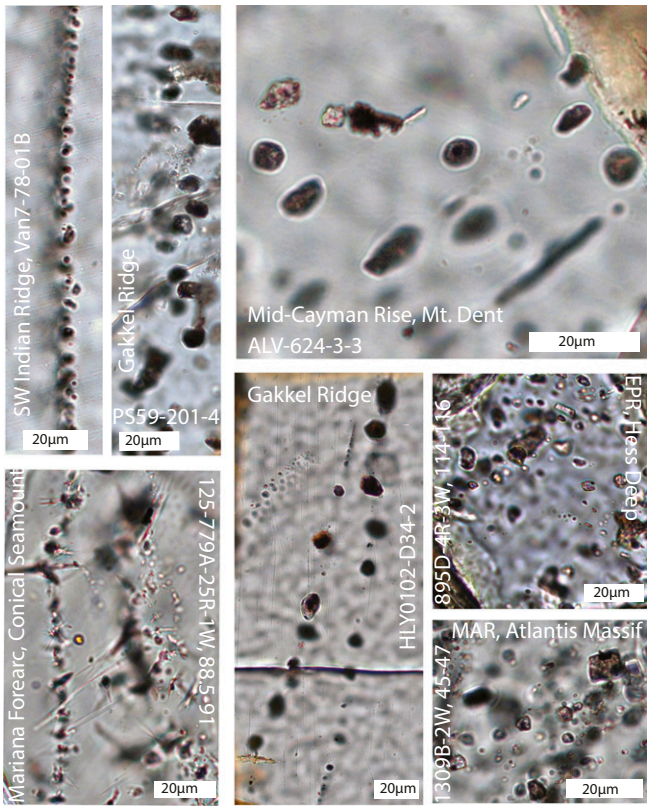

Fig. 2. Representative thin section photomicrographs of olivine-hosted fluid inclusions from the Southwest (SW) Indian Ridge, Gakkel Ridge, Mid-Cayman Rise (MCR), Mariana forearc (Conical Seamount), Hess Deep (East Pacific Rise, EPR), and the Mid-Atlantic Ridge (MAR, Atlantis Massif). Depicted inclusions contain serpentine, brucite, and magnetite, as well as $H_{2(g)}$ or $CH_{4(g)}$ or both as determined with confocal Raman spectroscopy.

compositions indicative of interactions with evolved seawater at temperatures up to 600 °C (17). Likewise, seawater may also be the principal source of trapped fluids in rocks from other midocean ridges and passive margins. In samples from subduction zone forearcs, in contrast, water trapped in olivine may be derived from devolatilization of the subducting slab (18–20).

The temperature range of fluid entrapment can be estimated using geodynamic and thermodynamic constraints. The upper temperature limit for entrapment of aqueous fluids in olivine (not hydroxyl in the crystal lattice) is its brittle–ductile transition temperature, which, depending on pressure, varies from 600 to 800 °C (21). At higher temperatures, olivine undergoes ductile deformation without fracturing, and aqueous fluids cannot efficiently penetrate olivine (22). Hydrogen- and CH_4-rich fluid inclusions occur in olivine-bearing rocks from midocean ridges, a backarc basin, and subduction zones (Fig. 1). The common element of these fundamentally different tectonic settings is the presence of aqueous fluids that percolate through fractured olivine-bearing rocks at high temperatures. What sets them apart is their distinct thermal structures, which affect the depth distribution of conditions favorable for secondary fluid-inclusion formation. At midocean ridges where geothermal gradients are steep, temperatures of 600 to 800 °C correspond to depths of ∼2 to 8 km where fluid-inclusion formation would be favorable. Secondary fluid-inclusion formation may occur at significantly greater depths where geothermal gradients are shallower, such as at magma-poor midocean ridges, ridge-flank environments, fracture zones, passive margins, and subduction zones (23, 24).

Fluids percolating through microfractures can only be trapped as secondary inclusions if the fractured mineral is thermodynamically stable and can anneal (9). We used the thermodynamic modeling code EQ3/6 (25) to assess the thermodynamic stability of olivine and the interactions between trapped fluids and the olivine host responsible for the formation of reaction products observed within inclusions as a function of temperature and $CO_{2(aq)}$ concentration (Fig. 4*A*). To this end, olivine ($Mg_{1.8}Fe_{0.2}SiO_4$) was reacted with an evolved seawater-like aqueous fluid in a 5:1 mass ratio at 100 MPa between 600 and 25 °C. Aqueous solutions initially contained 0.1, 1, or 10 mmol/kg $CO_{2(aq)}$ to assess how $\sum CO_2$ concentrations affect CH_4 formation.

Thermodynamic models (Fig. 4*A*) and hydrothermal experiments (26) suggest that Mg-rich olivine is stable in the presence of water at temperatures higher than ∼400 °C, which represents the approximate minimum temperature for fluid-inclusion formation. Note that the temperature stability of olivine in the presence of water is affected by its fayalite content and pressure (16). When the olivine host cools below ∼400 °C, it reacts with trapped water to form serpentine and magnetite. Only a small amount of olivine needs to dissolve for the trapped aqueous fluid to reach equilibrium with serpentine and olivine, according to the following generalized reaction for Mg end members:

$$\underset{\text{olivine}}{3Mg_2SiO_4} + 2H_2O + SiO_{2(aq)} = \underset{\text{serpentine}}{2Mg_3Si_2O_5(OH)_4}. \quad [1]$$

The limited extent of reaction **1** between 400 and 340 °C is illustrated by the negligible decrease in the mass of water present within the inclusion (blue line in Fig. 4*A*). When the olivine host cools below 340 ± 20 °C, brucite becomes part of the equilibrium mineral assemblage (Fig. 4*A*) according to the simplified reaction

$$\underset{\text{olivine}}{2Mg_2SiO_4} + 3H_2O = \underset{\text{serpentine}}{Mg_3SiO_4(OH)_2} + \underset{\text{brucite}}{Mg(OH)_2}. \quad [2]$$

Reaction **2** buffers the activity of water for a given temperature, pressure, and activities of olivine, serpentine, and brucite. The equilibrium constant of reaction **2** increases by 8 orders of magnitude between 340 and 25 °C. Assuming that the activities of olivine, serpentine, and brucite remain constant within the inclusion, the decrease of the equilibrium constant requires a decrease in water activity from approximately unity at 340 °C to 10^{-3} at 25 °C to maintain thermodynamic equilibrium (*SI Appendix*, Fig. S6). Because fluid inclusions represent a closed system and the

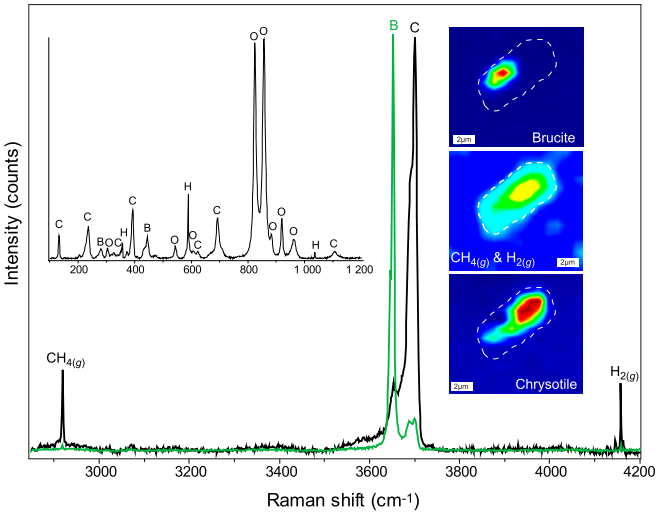

Fig. 3. Representative Raman spectra and hyperspectral Raman maps of an olivine-hosted inclusion in sample 107–651A-58R-1W, 48–50 recovered during Ocean Drilling Program Leg 107 from the Tyrrhenian Sea backarc basin. Abbreviations: C = chrysotile, B = brucite, O = olivine, H = hydrogen.

amount of trapped water inside an inclusion is small relative to the amount of olivine, reaction **2** can proceed until liquid water trapped in the inclusion is exhausted.

The water-driven oxidation of ferrous iron in olivine to ferric iron in magnetite and serpentine yields H_2, as represented by the generalized reaction

$$2FeO + H_2O = Fe_2O_3 + H_2, \quad [3]$$

where FeO and Fe_2O_3 represent the ferrous iron component of olivine and the ferric iron components of magnetite and serpentine, respectively. Consequently, fluids within the inclusion interior become increasingly H_2-rich as serpentinization proceeds. The model predicts the highest H_2 yields at ~300 °C (Fig. 4*A*) when the amount of magnetite present in the equilibrium mineral assemblage reaches a maximum (16). Indeed, the presence of magnetite and Fe contents of serpentine and brucite (*SI Appendix*, Fig. S5 and Table S2) suggest serpentinization temperatures of 250 to 300 °C within the inclusions (16). Confocal Raman spectroscopy revealed the presence of $H_{2(g)}$ in numerous olivine-hosted secondary fluid inclusions (Fig. 3 and *SI Appendix*, Figs. S1, S2, and S4 and Table S1), which is consistent with fluid mineral equilibria involving the mineral assemblage pentlandite-awaruite-magnetite detected in sample PS59-201–4 (27). As more H_2 is generated and water activity decreases, conditions become increasingly favorable for the reduction of $\sum CO_2$ to CH_4 (Fig. 4*A*) according to the reaction

$$\sum CO_2 + 4H_2 = CH_4 + 2H_2O. \quad [4]$$

Water generated by reaction **4** is available to serpentinize olivine via reactions **2** and **3**, while the concurrent consumption of H_2 promotes Fe oxidation via reaction **3**, thus contributing to the alteration of olivine. Together these reactions can proceed until H_2O or $\sum CO_2$ is exhausted. The equilibrium models in Fig. 4*A* predict an increase in $CH_{4(g)}$ fugacity with increasing initial $CO_{2(aq)}$ concentration at the time of entrapment. The model also suggests that $CH_{4(g)}$ formation is thermodynamically favorable if a $\sum CO_2$-bearing aqueous fluid trapped in olivine experiences cooling below 400 °C. Accordingly, the lack of detectable CH_4 in H_2-rich fluid inclusions from tectonic windows such as Hess Deep may reflect the absence of CO_2 in trapped fluids.

The strong temperature dependence of C speciation also implies a compositional depth stratification of olivine-hosted secondary fluid inclusions, with $CO_{2(aq)}$ as the dominant C species in deeper zones of the oceanic crust where temperatures exceed 400 °C and $CH_{4(g)}$ as the dominant C species in shallower zones where temperatures are lower. In ophiolites, present-day temperatures are much too low for fluid-inclusion formation to be currently ongoing at depth, suggesting that all olivine-hosted fluid inclusions formed in the geologic past either prior to obduction or during a later reheating event.

Abiotic CH_4 from Fluid Inclusions in Submarine and Subaerial Vent Systems

Recent radiocarbon and stable carbon isotope measurements, as well as mass-balance constraints of dissolved carbon species, suggest that abiotic CH_4 is not formed at the expense of $\sum CO_2$ during convection of submarine hydrothermal fluids (2–4). A magmatic source of abiotic CH_4 also seems unlikely since the upper mantle at midocean ridges is too oxidized to stabilize CH_4, and CH_4 from deeper sections in the mantle would "reequilibrate" to CO_2 and H_2O upon adiabatic decompression (28). As the present study demonstrates, olivine-hosted secondary fluid inclusions rich in CH_4 are widespread in the lower oceanic crust and upper mantle formed at midocean ridges. Leaching of olivine-hosted fluid inclusions represents a mechanism for the addition of abiotic CH_4 to circulating hydrothermal fluids in submarine serpentinization systems that is not at odds with available geological and geochemical constraints (2, 3, 6). Methane trapped in fluid inclusions has carbon isotopic compositions consistent with those of abiotic CH_4 in submarine serpentinization systems (6). Because CH_4 is formed in isolation from circulating vent fluids, the carbon required for CH_4 formation is not derived from circulating fluids, in keeping with measured vent fluid compositions (3). Moreover, CH_4 may be trapped within fluid inclusions for geologically significant periods of time resulting in a radiocarbon-poor CH_4 reservoir within the oceanic crust. Leaching of this CH_4 would account for the occurrence of radiocarbon-poor abiotic CH_4 in submarine hydrothermal fluids associated with serpentinization (3, 4). Together, these observations support the idea that olivine-hosted fluid inclusions represent a potentially significant source of abiotic CH_4 in submarine hydrothermal systems influenced by serpentinization.

Fluid inclusions in submarine serpentinization systems may also represent a source of abiotic CH_4 in mafic-hosted submarine hydrothermal systems that access gabbroic rocks. Fluids venting from mafic-hosted hydrothermal systems are typically characterized by much lower CH_4 concentrations than fluids venting from serpentinite-hosted hydrothermal systems. The large difference in concentrations notwithstanding, fluids from both environments show remarkably similar carbon isotopic compositions (2–4, 29, 30). The isotopic similarity points to a common underlying process responsible for CH_4 formation in these diverse substrates (2, 3). In this respect, it is important to note that serpentinization within olivine-hosted fluid inclusions in gabbro creates conditions conducive to CH_4 formation that are independent of the redox conditions in the surrounding rock and percolating fluids. Deeply penetrating hydrothermal fluids interacting with fluid-inclusion–bearing gabbro would have the same compositional features as fluids interacting with basalt, but be enriched in CH_4. Indeed, fluids venting from the mafic-hosted Menez Gwen hydrothermal system exhibit $CH_{4(aq)}$ concentrations of up to 2.15 mmol/kg despite having many compositional features typical of mafic-hosted systems such as relatively high $SiO_{2(aq)}$ and low $H_{2(aq)}$ concentrations (30). Methane in fluids venting from mafic-hosted hydrothermal systems that have similar carbon isotopic compositions, but lower concentrations (29), may reflect more limited access to gabbroic rocks in the underlying plumbing systems. The emerging picture suggests that fluid inclusions represent a significant source of abiotic CH_4 in both mafic-hosted and ultramafic-hosted submarine hydrothermal systems.

Olivine-hosted secondary fluid inclusions were found in all continental field locations indicated in Fig. 1. From these field areas, active venting of CH_4 has been documented at Zambales (1) and in the Ligurian Alps (31). As is the case for submarine hydrothermal systems, derivation of abiotic CH_4 by leaching from fluid inclusions is consistent with available constraints in continental serpentinization sites. Helium isotopes and stable carbon isotopic compositions of CH_4 in fluid inclusions overlap with those measured at continental CH_4 seeps (1, 6). Moreover, fluid inclusions were formed in the distant geological past (>50 ka) and therefore CH_4 is likely radiocarbon-free, as is observed in CH_4 from continental seeps (1). Olivine-hosted fluid inclusions from continental peridotites examined in this study show a range of CH_4 pressures with some of the highest (55 MPa) in the entire sample collection (*SI Appendix*, Table S1). Based on the results of this study, we can assess whether abiotic CH_4 trapped in fluid inclusions can account for the quantities of CH_4 released from continental seeps. For instance, the Chimaera serpentinization system in Turkey has released 0.076 to 0.5 km^3 CH_4 during the past 2 millennia (32, 33). If a source rock volume of 12 km^3 (32) is assumed, and that peridotite at Chimaera contains 75 wt. % olivine, the CH_4 abundances of 2.5 to 363 nmol $CH_{4(g)}$ per gram of olivine in peridotite would yield 0.002 to 0.26 km^3 of fluid-inclusion–derived CH_4, broadly consistent with the amounts of CH_4 released at Chimaera (*SI Appendix*, Fig. S7).

An alternative model involving CO_2 reduction via Sabatier reactions in gas-filled fractures, with requisite radiocarbon-free CO_2 derived from nearby sediments, has been proposed by Etiope and Whiticar (33) for the origin of abiotic CH_4 in continental serpentinization systems such as Chimaera and Zambales

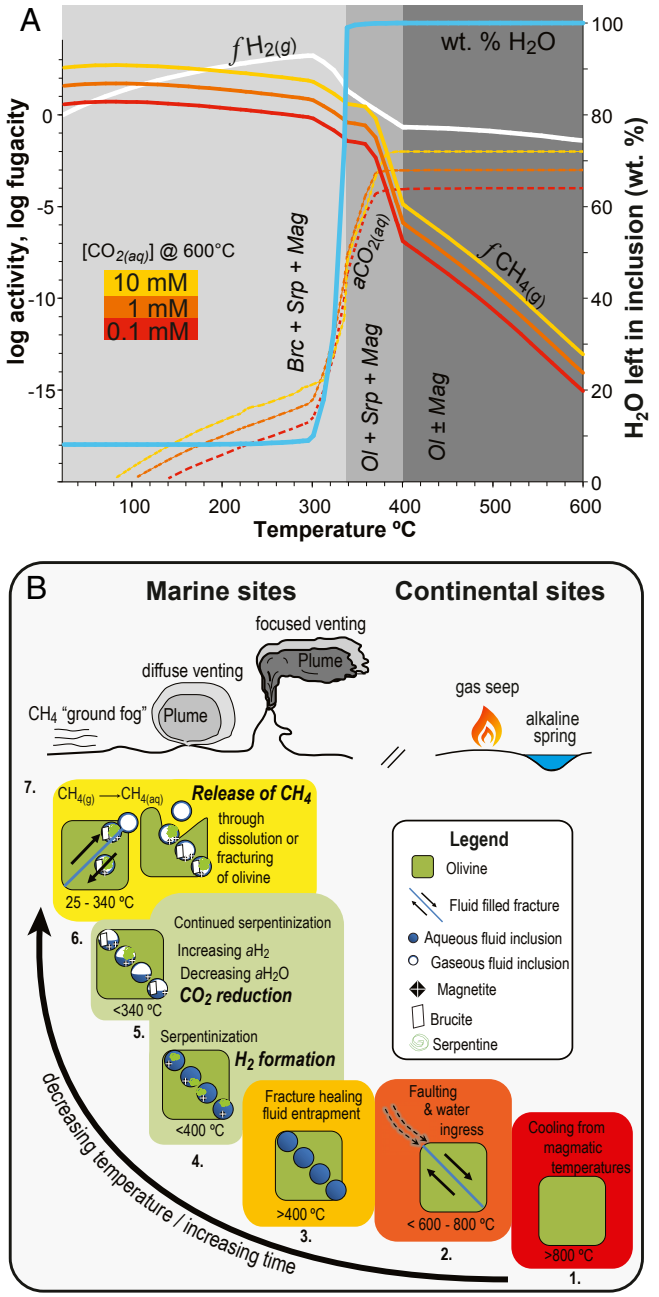

Fig. 4. Equilibrium model (*A*) and conceptual model (*B*) of CH_4 formation in olivine-hosted fluid inclusions. (*A*) Predicted equilibrium composition of a trapped fluid interacting with its olivine host in a closed system as a function of temperature and initial $CO_{2(aq)}$ concentration (0.1 to 10 mM). Also shown is the mass of reactant water as a function of temperature. Above ~400 °C, olivine (Ol) is stable, $CO_{2(aq)}$ is the dominant carbon species, and virtually none of the liquid water is consumed by hydrous minerals. Below ~340 °C, brucite (Brc), serpentine (Srp), and magnetite (Mag) form at the expense of olivine (unstable), and most of the water is consumed while abundant $H_{2(g)}$ and $CH_{4(g)}$ are formed. See *Methods* for modeling details. (*B*) Conceptual model illustrating the sequence of events that lead to the formation of CH_4 in olivine-hosted inclusions and its subsequent release. Cooling from magmatic temperatures (1) to below the brittle–ductile transition temperature (2) allows water to penetrate the rock. Healing of fluid-filled fractures (3) forms secondary fluid inclusions. During cooling below 400 °C, serpentinization begins (4). During cooling below 340 °C, increased H_2 generation and consumption of water create conditions conducive to CH_4 formation (5). Fracturing or dissolution of the olivine host releases volatiles (6), which subsequently vent at the surface (7).

(Philippines). These authors dismissed a fluid-inclusion–leaching model as a significant source of CH_4 at Chimaera based on mass balance estimates that indicated 5×10^3 km^3 peridotite would be required to produce 0.5 km^3 CH_4 from fluid inclusions, an unrealistic value considering the volume of peridotite at Chimaera is only ~12 km^3 (32). However, the foundation of Etiope and Whiticar's (33) calculation is the assumption that the internal gas pressure within fluid inclusions is 0.1 MPa (atmospheric pressure). Our results show that this is clearly not the case. Repeating their calculation and assuming internal CH_4 partial pressures of 0.4 to 55 MPa determined here would yield a required rock volume of 210 to 1.53 km^3 to account for the lower estimate of 0.076 km^3 CH_4 and 1,383 to 10.06 km^3 to account for the upper limit of 0.5 km^3 CH_4. Considering the large degree of overlap between the estimated amount of CH_4 venting at Chimaera and that in fluid inclusions, with the potential of excess CH_4 from fluid inclusions, there is little justification to preclude fluid inclusions as a source of CH_4 at Chimaera.

Summary and Implications

The findings presented in this study are summarized in a conceptual model involving 6 stages that account for venting of abiotic CH_4 at submarine and subaerial sites (Fig. 4*B*). Cooling of olivine-bearing rocks from magmatic temperatures to below the brittle–ductile transition (stage 1) is followed by faulting due to tectonic movements or thermal contraction, which allows ingress and entrapment of aqueous fluids (stages 2 and 3). Continued cooling causes serpentinization of the fluid-inclusion walls, H_2 generation, and water consumption, which creates conditions conducive to CO_2 reduction to abiotic CH_4 (stages 4 and 5). Subsequent interaction of the olivine host with percolating aqueous fluids or brittle fracturing releases abiotic CH_4 to circulating hydrothermal fluids (stage 6) that result in its transport to seafloor or subaerial vent sites. Venting of fluids enriched in abiotic CH_4 (stage 7) can occur via focused, diffuse, or nearly invisible "stealth" flow in both seafloor settings (3, 29, 34) and alkaline springs on land.

Most inclusions examined in this study occur in rocks collected at or near modern plate margins (Fig. 1) and have Quaternary cooling ages. In contrast, samples from the Zambales, Ligurian, and Josephine ophiolites are significantly older. The oldest CH_4-bearing sample examined in this study is a peridotite from the Josephine ophiolite that has not been heated since obduction during the Jurassic (35). These rocks demonstrate that, once formed, $CH_{4(g)}$ can be stored in olivine-hosted fluid inclusions over geological timescales.

The formation of H_2 and CH_4 in olivine-hosted secondary inclusions has likely been occurring since the onset of plate tectonics. Extraction of trapped volatiles may have supported microbial ecosystems within diverse geologic environments (Fig. 1). An intriguing aspect of H_2 and CH_4 formation in fluid inclusions is that these reduced volatiles can be stored over geological timescales and extracted at a later point in time, even after hydrothermal activity has ceased or when liquid water is no longer present. Such a process may be particularly relevant to sources of CH_4 on Mars where spikes in atmospheric CH_4 have been reported (36) and recently confirmed (37), even though Mars has lost much of its atmosphere and liquid water. Furthermore, if Mars is still seismically active (38), CH_4 could be extracted through continual or episodic fracturing of the host rock.

Present-day release of trapped volatiles by these mechanisms may provide sufficient H_2 and CH_4 to supply microbial ecosystems with electron donors in natural environments where H_2 or CH_4 formation would otherwise not be favorable. On ice-covered moons such as Europa and Enceladus, where liquid water may interact with an olivine-bearing rocky core, present-day conditions may be conducive to the ongoing formation of fluid inclusions, particularly if olivine is iron-rich. High iron contents can increase the stability of olivine in the presence of water, thus lowering the minimum temperature of fluid inclusion formation to as low as 200 °C (16).

Results of this study demonstrate the presence of olivine-hosted fluid inclusions in a broad array of geological settings. Extrapolation of our results globally suggests that inclusions may

represent one of the largest sources of abiotic CH_4 on Earth. Circulation of aqueous fluids in olivine-rich substrates is critical in the formation of fluid inclusions, in the release of CH_4 from fluid inclusions, and in the transport of CH_4 to vent sites where it is available to participate in numerous biogeochemical processes. Similar processes involving fluid inclusions may occur elsewhere in the solar system, with important implications for the distribution and maintenance of microbial life beyond Earth.

Methods

Thin sections were examined for fluid inclusions using a petrographic microscope. Reflected light microscopy was used to locate and examine opened inclusions. Fluid-inclusion abundances were estimated by analyzing back-scattered electron images of inclusions exposed by polishing. The mineral and volatile contents of secondary fluid inclusions were studied with a Horiba LabRam HR800 confocal Raman microscope equipped with 3 lasers (473, 532, and 633 nm), a motorized x-y-z stage, 2 gratings (600 and 1,800 grooves per millimeter), and a thermoelectric-cooled charge-coupled detector (1,024 × 256 pixels). The system was calibrated daily using a silicon wafer and a monochromatic neon light source (Oriel model 6032). We chose a 473-nm laser and a 100× objective (numerical aperture = 0.9) to resolve objects smaller than 0.6 μm. To achieve the highest possible spectral resolution for CH_4 pressure calculations using Raman band position measurements (11), we chose a 633-nm laser, a grating with 1,800 grooves per millimeter, and a slit size of 30 μm. Acquisition times ranged from 5 to 60 s per analysis. To improve signal-to-noise ratios, 3 to 5 acquisitions were averaged. Spectra were processed with the LabSpec 6 software for background correction using polynomial functions and for peak fitting using a pseudo-Voigt function. In addition to spot analysis, we acquired hyperspectral Raman maps using a 473-nm laser, 600 grooves per millimeter grating, 100 to 300 μm confocal hole diameter, 1 to 30 s acquisition time, 1 to 3 accumulation(s) per spot, and x-y step sizes of 0.5 to 2 μm. Hyperspectral Raman maps were further processed with the multivariate data analysis module integrated in the LabSpec 6 software. Measured and calculated end-member spectra were compared with reference spectra (11, 39–41).

Field-emission scanning electron microscopy (Marine Biological Laboratory) and electron microprobe analysis (FE-EMPA, Yale University) were used to examine open fluid inclusions that were exposed by careful polishing. FE-EMPA was carried out using an accelerating voltage of 15 kV and a beam current of 10 nA. Spot sizes for quantitative analyses of hydrous minerals were at least 3.5 μm to minimize beam damage. The beam was fully focused for magnetite, sulfide, and alloy measurements. Natural and synthetic standards were used for element calibration, and raw data were corrected using the Phi-Rho-Z method (42).

Fluid-inclusion analyses were complemented with thermodynamic equilibrium models for reactions between trapped aqueous fluids and the olivine host as a function of temperature and CO_2 concentration using the software code EQ3/6 (25). We used a customized thermodynamic database (16), which includes equilibrium constants calculated with the software code SUPCRT92 (43) for a temperature range of 25 to 600 °C at a constant pressure of 100 MPa. Olivine ($Mg_{1.8}Fe_{0.2}SiO_4$) was used as the solid starting material in all models. The salinity of the aqueous fluid was adjusted to 3.5‰, which allowed computation of equilibrium models with ionic strengths of <0.04 and water activities close to unity at water-to-olivine mass ratios of 0.2. The low water-to-olivine ratio was chosen to model reactions involving a small amount of fluid trapped in a large amount of olivine.

ACKNOWLEDGMENTS. We are indebted to J. Eckert for his support with FE-EMPA; to K. Aquinho and E. Codillo for providing samples from Zambales; to K. Aquinho for Raman analysis of some of the samples from Zambales and Mt. Dent; to H. Dick for providing access to his thin section collection; to the curators of the IODP core repositories for providing access to Ocean Drilling Program (ODP) and Integrated Ocean Drilling Program (IODP) samples; and to the captains and crews of the many cruises without whom the collection of these samples would not have been possible. Reviews by Peter Kelemen and an anonymous referee greatly improved this manuscript. This study is supported with funds provided by the National Science Foundation (NSF-OCE Award 1634032 to F.K. and J.S.S.).

1. T. A. Abrajano *et al*., Geochemistry of reduced gas related to serpentinization of the Zambales ophiolite, Philippines. *Appl. Geochem.* **5**, 625–630 (1990).
2. D. T. Wang, E. P. Reeves, J. M. McDermott, J. S. Seewald, S. Ono, Clumped isotopologue constraints on the origin of methane at seafloor hot springs. *Geochim. Cosmochim. Acta* **223**, 141–158 (2018).
3. J. M. McDermott, J. S. Seewald, C. R. German, S. P. Sylva, Pathways for abiotic organic synthesis at submarine hydrothermal fields. *Proc. Natl. Acad. Sci. U.S.A.* **112**, 7668–7672 (2015).
4. G. Proskurowski *et al*., Abiogenic hydrocarbon production at lost city hydrothermal field. *Science* **319**, 604–607 (2008).
5. E. L. Shock, "Chemical environments of submarine hydrothermal systems" in *Marine Hydrothermal Systems and the Origin of Life*, N. G. Holm, Ed. (Kluwer Academic, Dordrecht, 1992), pp. 67–107.
6. N. G. Grozeva, "Carbon and mineral transformations in seafloor serpentinization systems," PhD thesis, Massachusetts Institute of Technology, Cambridge, MA (2018).
7. D. S. Kelley, G. L. Früh-green, Volatile lines of descent in submarine plutonic environments: Insights from stable isotope and fluid inclusion analyses. *Geochim. Cosmochim. Acta* **65**, 3325–3346 (2001).
8. D. A. Vanko, D. S. Stakes, *Fluids in Oceanic Layer 3: Evidence from Veined Rocks, Hole 735B, Southwest Indian Ridge*, R. P. Von Herzen, P. T. Robinson, Eds. (Proceedings of the Ocean Drilling Program Scientific Results, Ocean Drilling Program, College Station, TX, 1991), pp. 181–215.
9. E. Roedder, *Fluid Inclusions* (Mineralogical Society of America, Washington, DC, 1984).
10. H. M. Lamadrid *et al*., Effect of water activity on rates of serpentinization of olivine. *Nat. Commun.* **8**, 16107 (2017).
11. W. Lu, I.-M. Chou, R. C. Burruss, Y. Song, A unified equation for calculating methane vapor pressures in the CH_4–H_2O system with measured Raman shifts. *Geochim. Cosmochim. Acta* **71**, 3969–3978 (2007).
12. R. L. Carlson, The abundance of ultramafic rocks in Atlantic Ocean crust. *Geophys. J. Int.* **144**, 37–48 (2001).
13. M. Cannat, How thick is the magmatic crust at slow spreading oceanic ridges? *J. Geophys. Res.* **101**, 2847–2857 (1996).
14. H. J. A. Van Avendonk, J. K. Davis, J. L. Harding, L. A. Lawver, Decrease in oceanic crustal thickness since the breakup of Pangaea. *Nat. Geosci.* **10**, 58 (2016).
15. C. MacFarling Meure *et al*., Law Dome CO_2, CH_4 and N_2O ice core records extended to 2000 years BP. *Geophys. Res. Lett.* **33**, L14810 (2006).
16. F. Klein, W. Bach, T. M. McCollom, Compositional controls on hydrogen generation during serpentinization of ultramafic rocks. *Lithos* **178**, 55–69 (2013).
17. E. Ito, R. N. Clayton, Submarine metamorphism of gabbros from the Mid-Cayman rise: An oxygen isotopic study. *Geochim. Cosmochim. Acta* **47**, 535–546 (1983).
18. L. H. Rüpke, J. P. Morgan, M. Hort, J. A. D. Connolly, Serpentine and the subduction zone water cycle. *Earth Planet. Sci. Lett.* **223**, 17–34 (2004).
19. S. Arai, H. Hirai, Relics of H_2O fluid inclusions in mantle-derived olivine. *Nature* **318**, 276–277 (1985).
20. S. Arai, S. Ishimaru, T. Mizukami, Methane and propane micro-inclusions in olivine in titanoclinohumite-bearing dunites from the Sanbagawa high-P metamorphic belt, Japan: Hydrocarbon activity in a subduction zone and Ti mobility. *Earth Planet. Sci. Lett.* **353–354**, 1–11 (2012).
21. G. D. Harper, Tectonics of slow spreading mid-ocean ridges and consequences of a variable depth to the brittle/ductile transition. *Tectonics* **4**, 395–409 (1985).
22. S. Rouméjon, M. Cannat, Serpentinization of mantle-derived peridotites at mid-ocean ridges: Mesh texture development in the context of tectonic exhumation. *Geochem. Geophys. Geosyst.* **15**, 2354–2379 (2014).
23. V. Schlindwein, F. Schmid, Mid-ocean-ridge seismicity reveals extreme types of ocean lithosphere. *Nature* **535**, 276–279 (2016).
24. E. M. Syracuse, P. E. van Keken, G. A. Abers, The global range of subduction zone thermal models. *Phys. Earth Planet. Inter.* **183**, 73–90 (2010).
25. T. J. Wolery, EQ3/6, A Software Package for Geochemical Modeling of Aqueous Systems: Package Overview and Installation Guide (Version 7.0, Lawrence Livermore National Laboratory, Livermore, CA, 1992).
26. D. E. Allen, W. E. Seyfried Jr, Compositional controls on vent fluids from ultramafic-hosted hydrothermal systems at mid-ocean ridges: An experimental study at 400°C, 500 bars. *Geochim. Cosmochim. Acta* **67**, 1531–1542 (2003).
27. F. Klein, W. Bach, Fe-Ni-Co-O-S phase relations in peridotite seawater interactions. *J. Petrol.* **50**, 37–59 (2009).
28. E. Cottrell, K. A. Kelley, The oxidation state of Fe in MORB glasses and the oxygen fugacity of the upper mantle. *Earth Planet. Sci. Lett.* **305**, 270–282 (2011).
29. J.-L. Charlou, J.-P. Donval, Y. Fouquet, P. Jean-Baptiste, N. Holm, Geochemistry of high H_2 and CH_4 vent fluids issuing from ultramafic rocks at the Rainbow hydrothermal field (36°14′N, MAR). *Chem. Geol.* **191**, 345–359 (2002).
30. J. L. Charlou *et al*., Compared geochemical signatures and the evolution of Menez Gwen 37°50′N and Lucky Strike 37°17′N hydrothermal fluids, south of the Azores Triple Junction on the Mid-Atlantic Ridge. *Chem. Geol.* **171**, 49–75 (2000).
31. M. Quéméneur *et al*., Endolithic microbial communities in carbonate precipitates from serpentinite-hosted hyperalkaline springs of the Voltri Massif (Ligurian Alps, Northern Italy). *Environ. Sci. Pollut. Res. Int.* **22**, 13613–13624 (2015).
32. H. Hosgormez, G. Etiope, M. N. Yalçin, New evidence for a mixed inorganic and organic origin of the Olympic Chimaera fire (Turkey): A large onshore seepage of abiogenic gas. *Geofluids* **8**, 263–273 (2008).
33. G. Etiope, M. J. Whiticar, Abiotic methane in continental ultramafic rock systems: Towards a genetic model. *Appl. Geochem.* **102**, 139–152 (2019).
34. B. I. Larson *et al*., Stealth export of hydrogen and methane from a low temperature serpentinization system. *Deep Sea Res. Part II Top. Stud. Oceanogr.* **121**, 233–245 (2015).
35. A. J. Coulton, G. D. Harper, D. S. O'Hanley, Oceanic versus emplacement age serpentinization in the Josephine ophiolite: Implications for the nature of the Moho at intermediate and slow spreading ridges. *J. Geophys. Res. Solid Earth* **100**, 22245–22260 (1995).

36. C. R. Webster *et al.*; MSL Science Team, Mars atmosphere. Mars methane detection and variability at Gale crater. *Science* **347**, 415–417 (2015).
37. M. Giuranna *et al.*, Independent confirmation of a methane spike on Mars and a source region east of Gale Crater. *Nat. Geosci.* **12**, 326–332 (2019).
38. A.-C. Plesa *et al.*, Present-day Mars' seismicity predicted from 3-D thermal evolution models of interior dynamics. *Geophys. Res. Lett.* **45**, 2580–2589 (2018).
39. R. T. Downs, "The RRUFF project: An integrated study of the chemistry, crystallography, Raman and infrared spectroscopy of minerals" in *19th General Meeting of the International Mineralogical Association in Kobe, Japan* (International Mineralogical Association, Kobe, Japan, 2006), O03-13.
40. M. L. Frezzotti, F. Tecce, A. Casagli, Raman spectroscopy for fluid inclusion analysis. *J. Geochem. Explor.* **112**, 1–20 (2012).
41. J. R. Petriglieri *et al.*, Micro-Raman mapping of the polymorphs of serpentine. *J. Raman Spectrosc.* **46**, 953–958 (2015).
42. J. T. Armstrong, "Quantitative elemental analysis of individual microparticles with electron beam Instruments" in *Electron Probe Quantitation*, K. F. J. Heinrich, D. E. Newbury, Eds. (Springer US, Boston, 1991), pp. 261–315.
43. J. W. Johnson, E. H. Oelkers, H. C. Helgeson, SUPCRT92: A software package for calculating the standard molal thermodynamic properties of minerals, gases, aqueous species, and reactions from 1-5000 bars and 0-1000°C. *Comput. Geosci.* **18**, 899–947 (1992).